Journal of Molecular Liquids 343 (2021) 117598

Contents lists available at ScienceDirect

Journal of Molecular Liquids

journal homepage: www.elsevier.com/locate/molliq

# The design and green nanofabrication of noble hydrogel systems with encapsulation of doped bioactive hydroxyapatite toward sustained drug delivery

Ramón Rial [a,*], Natalia Hassan [b], Zhen Liu [c], Juan M. Ruso [a]

[a] Soft Matter and Molecular Biophysics Group, Department of Applied Physics, University of Santiago de Compostela, 15782 Santiago de Compostela, Spain
[b] Programa Institucional de Fomento a la I+D+i, Universidad Tecnológica Metropolitana, Ignacio Valdivieso 2409, San Joaquín, Santiago, Chile
[c] Department of Physics and Engineering, Frostburg State University, Frostburg, MD 21532, USA

ARTICLE INFO

*Article history:*
Received 16 July 2021
Revised 14 September 2021
Accepted 15 September 2021
Available online 20 September 2021

*Keywords:*
Microfluidics
Tissue engineering
Regenerative medicine
Hydrogels

ABSTRACT

Finding a bioactive hybrid material with the potential for a controlled drug release has been one of the major targets of tissue engineering in the recent years. In this line, the present work describes a new approach for producing singular hydrogel microparticles (HMPs) with different morphologies and compositions by combining experimental and computational methods. Calcium-Alginate microparticles (Ca-ALG) and core–shell Alginate-Chitosan microspheres (Ca-ALG-CHI) were synthesized with the presence of drug-doped Hydroxyapatite (HA) in their inner matrix. The methodology relies on the use of a microfluidic system to obtain crosslinked HMPs with homogeneous sizes and morphologies, integrating external and internal gelation. The impact of the water-to-oil volume ratio, as well as variations in the collecting baths, morphology, and dispersion, were considered. The drug models chosen were Propranolol hydrochloride and Cloxacillin sodium salt monohydrate. Avrami's parameters were used to study and address the adsorption kinetics of each drug onto the bioactive HA, and the Korsmeyer-Peppas model was used to analyze the posterior desorption profiles. The conception and development of this type of hydrogel microparticles with improved functionalities are essential for the creation of granular hydrogels, which are an innovative, green, sustained and highly promising solution for different therapies in regenerative medicine areas.



## 1. Introduction

In the past decade, there has been a rising interest in the study of inorganic nanoparticles in the field of medicine, due to their multiple functionalities. In particular, nanosized hydroxyapatite (HA) has attracted significant attention, as its chemical composition, improved biocompatibility and great mechanical properties, place it as a satisfactory solution for a wide variety of problems that require filling or coating of hard tissues. Furthermore, HA has the potential of being used as a drug carrier [1–3] and has also been effectively used for the sustained release of multiple antibiotic and anti-inflammatory drugs [4–7]; attributes that can be of a huge impact in partially alleviate or completely avoid some of the infections and diseases that could derive from orthopaedic implant surgeries. For their part, alginate (ALG) and chitosan (CHI) are natural polysaccharides derived from brown algae and from the partial deacetylation of chitin [8,9], respectively. Both compounds present great biocompatible and biodegradable properties, which added to their relatively low price and accessibility, make them especially appealing materials in the fields of tissue engineering and drug delivery systems [10–14]. Currently, some authors have focused on different combinations of them, with bone regeneration purposes [15–20]. Still, there is a wide room from improvement in the research and development of complex hybrid materials with advanced applications for bone and drug delivery.

Usually, hydrogels are created as continuous materials with its external dimensions in the macroscale and an internal mesh size in the nanoscale. It is also common to add a certain degree of porosity to their inner matrix, using different processing approaches [21]. Nevertheless, bulk hydrogels present disadvantages for certain applications like injection or extruded-based 3D printing. To address this question, the fabrication of hydrogel microparticles (HMPs) is gaining major attention, as they can be created from a wide diversity of synthetic or natural polymers and their shapes and morphologies can be adjusted according to the requirements.

* Corresponding author.
*E-mail address:* ramon.rial@usc.es (R. Rial).

https://doi.org/10.1016/j.molliq.2021.117598
0167-7322/

Among the most important properties of HMPs are: their inherently modular nature, allowing to create materials with mixed composition [22], the adjustability of the level of porosity, just by varying sizes and packing density [23], and, as exposed, their ability to flow through small needles or catheters.

There are different alternatives to fabricate HMPs depending on the materials or the crosslinking processes, namely: batch emulsions, lithography or mechanical fragmentation. Nevertheless, the application of microfluidic emulsions is the most effective in terms of the low dispersity indexes of particle populations obtained and its compatibility with particle, protein or drug encapsulation. The versatility, efficiency and the possibility of having a great control of the processes [24–26], has converted microfluidic technology in a growing discipline for multiple applications related to this field, like tissue engineering [27,28], drug encapsulation [29,30] chemical processing [31] or novel methods of synthesis [32].

As reported, the shape as well as the size and size distribution are crucial factors in properties like the rheology [33,34] or the biodistribution after intravascular injections [35]. The behaviour of spherical microparticles is more homogeneous and predictable than non-spherical ones, which will have a natural tendency to align or agglomerate in flowing processes [36]. Thus, if the desired material is thought to be used in 3D printing, injected through needles, in microcatheters, or in a similar technique of interventional therapy, microspheres are always the preferred choice [37]. Similarly, if the hydrogel has the potential to be used as a drug carrier, the lack of uniformity will lead to notable differences in thickness; which, ultimately, will produce uncertain and unstable release profiles [38]. Thereby this work presents a novel method, combining external and internal gelation. External gelation will be attained by means of two different external baths, and internal will be caused by the bonding formed between $Ca^{2+}$ present on the HA surface and the oxygen sites of $COO^-$ groups of ALG [39]. The idea is to obtain Ca-ALG microparticles and core–shell Ca-ALG-CHI microspheres with homogeneous sizes and morphologies and load them with doped HA. Propranolol hydrochloride (Prop) and cloxacillin sodium salt monohydrate (Clox) were used as the drug models. The adsorption kinetics for each drug onto bioactive HA has been studied and discussed using Avrami's parameters [40] and the posterior desorption profiles have been analysed through the Korsmeyer-Peppas model [41].

## 2. Materials and methods

### 2.1. Materials and reagents

Hexadecyl-trimethyl ammonium bromide (CTAB, ref. n. H6269, Sigma-Aldrich), polypropylene glycol (PPG, ref. n. 202304, Sigma-Aldrich), sodium phosphate, ($Na_3PO_4$, ref. n. 342483, Sigma-Aldrich), calcium chloride ($CaCl_2$, ref. n. C1016, Sigma-Aldrich), sodium nitrite ($NaNO_2$, ref. n. 237213, Sigma-Aldrich), Alginic acid sodium salt (ALG, ref. n. 180947, Sigma-Aldrich), Chitosan (CHI, ref. n. 448877, Sigma-Aldrich), Cloxacillin sodium salt monohydrate (Clox, ref. n. C9393, Sigma-Aldrich), Propranolol hydrochloride (Prop, ref, n, P-0884, Sigma-Aldrich), Acetic acid ($C_2H_4O_2$, ref. n. A6283, Sigma-Aldrich), Sodium acetate trihydrate ($C_2H_3NaO_2{\cdot}3H_2O$, ref. n. S8625, Sigma-Aldrich), Sunflower seed oil (S_Oil, maximum acidity 0.2°, commercial) were used without further purification. For solution preparation, only triple-distilled water was used.

### 2.2. Computational simulations

In order to anticipate and predict the behaviour of the two immiscible phases, COMSOL Multiphysics was used to model the droplet formation and study the dependence on the physical properties and the rates of the respective flows. This method involves the well-known procedure of modelling with finite elements [42]. In particular, in this study, the two-dimensional geometry was built respecting the real scale of the microfluidic chip as well as the angles of the channels in the intersection point. Three – dimensional structures were computationally built for visualization and representation purposes only. The corresponding values for density and viscosity of water and vegetable oil were used as provided in the database of the software, while the chosen surface tension was pre-set as corn oil/water (Results shown in Table 1). Even though it is true that the vegetable oil used in the laboratory assays was from sunflower seed origin, this configuration provided a more than adequate approximation. Mass balances were modelled by the Navier-Stokes equations and the interface of each fluid was calculated by a level set method [43]. This approach studies the evolution of the interface creating an isocontour curve of the level set function $\varphi$. In this case, the interface was set to $\varphi_{oil} = \varphi_{water} = 0.5$. Droplet diameter was obtained by the following expression:

$$d_s = 2\sqrt{\int_{\Omega} \frac{d\Omega}{\pi}} \quad (1)$$

Being $d_s$ the droplet diameter, and $\Omega$ the generating zone of a single droplet.

Calculations were run introducing fixed values for the normal velocity of the flow inlets, and the domain elements defined by the mesh were solved through Finite Element Method. As the study is time-dependent, the software required a time range, which in this particular case was from 0 to 3 s, with a time step of 0.02 s, to assure the convergence.

### 2.3. Microchip fabrication

The microfluidic devices were created by lithography. The mould was obtained by exposing a 2″ diameter silicon wafer to oxygen plasma to clean its surface, and then spin coating it with an epoxy resin at 500 rpm for 75 s to control the size of the channels. Under these conditions, square-section channels of 700 μm length were created. The solvent of the resin was removed by a pre-baking procedure carried out in a hot plate at 60 °C for 8 min and 95 °C for 15 min. When the resin solidified onto the substrate, a mask was placed and the resin was cross-linked by UV lamp (365 nm) for 4 min.

Next, the substrate was submerged in propylene glycol monomethyl ether acetate (PGMEA) for 10 min in order to discard the non-exposed resin of the substrate. Then, to achieve a better robustness of the mould, it was baked at 135 °C and 2 h. Afterward, polydimethylsiloxane (PDMS) was inserted into the generated mould and left for 45 min in an oven at 60 °C until complete solidification was achieved. Once the PDMS chips were obtained, the concluding step was to assemble them to the surface of microscopy

**Table 1**
Parameters used for simulations. Density and viscosity values obtained from the COMSOL material library. Interfacial tension from works by Fischer et al. [44].

| Parameter | Value |
|---|---|
| Density of water ($\rho_w$) | 999.62 kg/m$^3$ |
| Viscosity of water ($\eta_w$) | 0.0010 Pa·s |
| Density of oil ($\rho_O$) | 879.01 kg/m$^3$ |
| Viscosity of oil ($\eta_O$) | 0.0208 Pa·s |
| Contact angle | 108° |
| Interfacial tension ($\sigma$) | 0.0239 N/m |

slides. To do so, the surfaces of the slides were also covered with PDMS and cured. Then, both the chips and the slides were put in a plasma cleaner for 1 min to activate their surfaces. Once in contact, the microscope slides and the chips were merged correctly and consolidated, ending the process and obtaining the final microchips.

### 2.4. Preparation procedure for calcium alginate microparticles (Ca-ALG) and chitosan-covered microspheres (Ca-ALG-CHI)

To prepare the disperse phase, a known amount of sodium alginate was dissolved in triple distilled water for 3 h at 37 °C and 250 rpm, until obtaining a homogeneous and viscous solution with a 2 wt% concentration. This solution was pumped into the system through the first inlet (Fig. 1, inlet A).

For its part, crystalline hydroxyapatite-nanoparticles (HA), measuring 99 ± 16 nm length, were obtained by a method developed by us. The synthesis involves the use of a microfluidic system created *ad hoc* that allows controlling particle morphologies in real time and in a single step. A full description of the procedure can be found elsewhere [32]. Synthesized HA particles were drug-loaded as described below and dispersed in water with a concentration of 0.7 mg/ml. Then, they were introduced in the microchip through the following middle inlet (inlet B) in such a way that the particles were wrapped up by the alginate solution in the point P1 (Fig. 1), obtaining spherical microdroplets with drug-loaded nanoparticles in their centre. The continuous phase was inserted through the C and D side inlets (Fig. 1) and consisted of a solution of sunflower seed oil with 2 wt% Span 80 pre-dissolved. The use of this surfactant regulates the interfacial surface tension of the oil/water system, helping to obtain less fragile droplets and avoiding coalescence.

The inputs were attached to two syringe pumps (KDS 101 Legacy Syringe Pump) configured in such a way that allowed maintaining a precise and controlled flow in each inlet. After any modification in the flow rate of the oil or water phases, the system was stabilised for a minimum of 5 min in order to assure stationary state and to avoid instabilities or inhomogeneous flows, before removing droplets for gelation or for imaging.

In a typical experiment, doped HA–ALG droplets were formed inside the main channel of the microfluidic chip. These microdroplets were transferred through a silicone tube to the respective gelation baths. The end of this collecting tubing was maintained at the surface of the bath to avoid deformation on the dripping process. The collecting baths were composed by: 20 mL of a 20% (w/v) $CaCl_2$ water solution (to obtain Ca-ALG tear-shaped microparticles) or 20 mL of a 20% (w/v) $CaCl_2$ and 0.1% (w/v) Chitosan in a 1% (v/v) acetic acid solution (to obtain Ca-ALG-CHI core–shell microparticles). A period of 24 h was allowed for complete gelation before the synthesized microgel particles were further characterized.

### 2.5. Adsorption, kinetic and desorption processes and their assessment by means of models

The drug loading for both the active principles, Propranolol and Cloxacillin, was carried out by incubation of the HA nano-rods in solutions of the drugs for 7 days. Specifically, known amounts of Prop and Clox were weighed and dissolved in 20 mL of water to obtain initial concentrations ($C_0$) of 0.05 mM and 0.1 mM, respectively. Next, 3.5 mg of the nano-rods were added to the solutions and left at room temperature. At each time point, samples were centrifuged at 5000 rpm for 5 min and a small aliquot (3 mL) of the supernatant was collected. The concentrations of drug in the supernatant, $c_t$, were then determined by UV–Vis spectroscopy

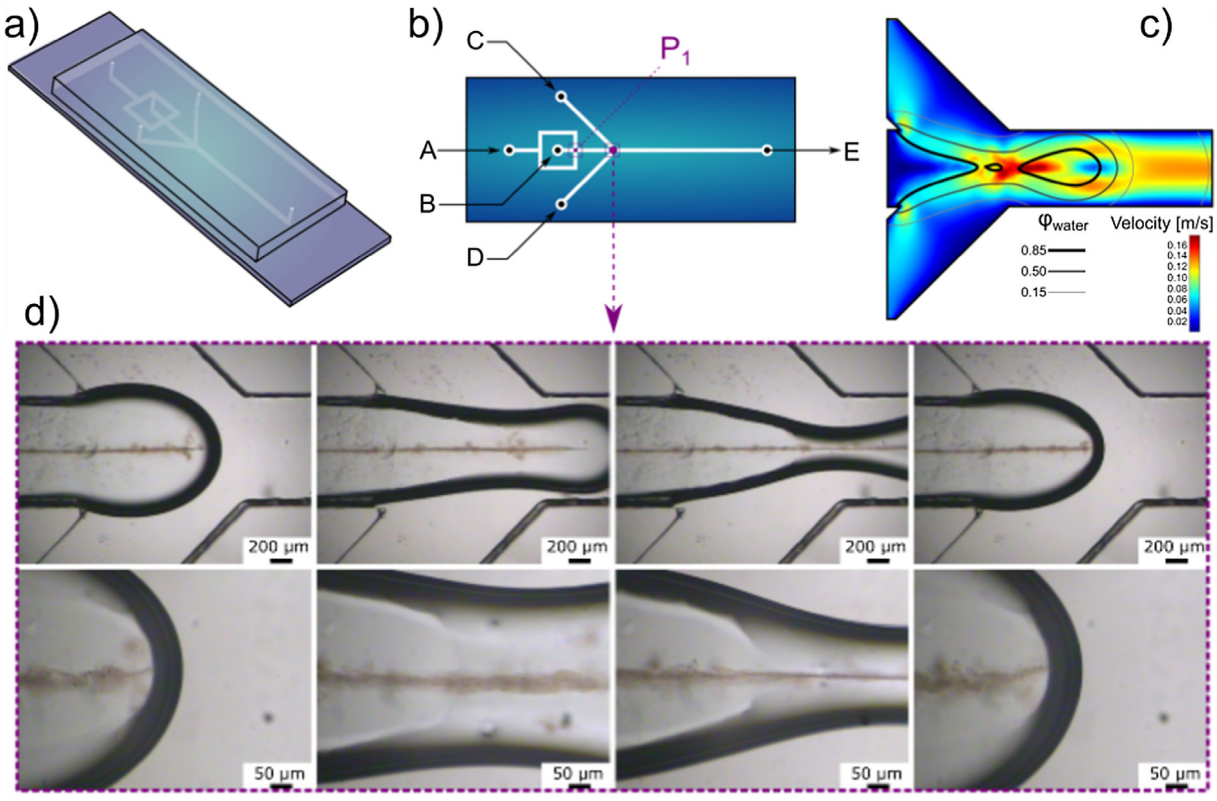


**Fig. 1.** a) Three-dimensional representation of the microfluidic device. b) Schematic representation. Geometry, inlets, outlets and significant points are depicted. c) Computational simulations results. d) Optical images. The continuous formation of the droplets as well as the nanoparticle flow can be tracked in this point.

(Cary 100 Bio UV–vis spectrophotometer) by measuring absorbance at $\lambda_{max}$, 290 nm for Prop [45] and 344 nm for Clox [46]. Standard curves in the concentrations range for each of the active ingredient were previously performed. Then, the adsorption kinetics was evaluated using Avrami's model.

Similarly, for the desorption studies, samples of loaded HA nano-rods, Ca-ALG microparticles and CaI-ALG-CHI microspheres were left in the same amount of media (triple distilled water) at room temperature and UV–Vis spectra of the supernatants were collected for each time point for 60 days. Finally, the results were fitted to the Korsmeyer-Peppas model.

The adsorption quality of the drugs was determined by the following expression:

$$Q_t = \frac{(c_0 - c_t) \cdot V}{m} \tag{2}$$

where $Q_t$ is the amount of drug adsorbed on HA nanoparticles ($mmol \cdot g^{-1}$), $c_o$ and $c_t$ are the initial and residual concentrations of the drugs in the supernatant at time t (mM), respectively; V is the volume of the drug solutions (L), and m is the mass of HA added (g).

### 2.6. Loading and release efficacy

The adsorbed and released percentages for both drugs were obtained as follows:

$$L_{AI}\% = \frac{[AI]_i - [AI]_f}{[AI]_i} \times 100 \tag{3}$$

$$R_{AI}\% = \frac{[AI]_i}{[AI]_a} \times 100 \tag{4}$$

$$[AI]_a = [AI]_i - [AI]_f \tag{5}$$

Being, $[AI]_a$ and $[AI]_l$ the adsorbed and released concentration of active ingredient (Prop or Clox), $L_{AI}$% and $R_{AI}$% the percentage of the active ingredient, adsorbed onto the hydroxyapatite nano-rods and released, respectively, and $[AI]_i$ , $[AI]_f$ the initial and final supernatant concentration of active ingredient in which HA nano-rods were incubated.

## 3. Results and discussion

### 3.1. Flow simulations and influence of flow rates on the microdroplet generation

When two immiscible liquids are in contact, they maintain their interphase as small as possible, due to the natural tendency of substances to keep the minimal energy on the surface. This physical phenomenon plays a crucial role in the process of emulsification, in which an immiscible liquid gets dispersed in another insolvable fluid by the formation of droplets. To analyse and study the emulsification process under different conditions COMSOL software was used. The two-phase flow simulation results as well as their experimental counterparts are shown in Fig. 2. The volume fraction of the two phases is represented, being the blue colour corresponding to $\varphi_{oil} = 1$, red corresponding to pure water phase and light green to the interphase or $\varphi_{oil} = \varphi_{water} = 0.5$.

Results of the simulations show a clear relation between velocity, size and rate of droplet formation. As the continuous phase flow increases, the viscous shear-stress augments, overcoming interfacial tension and "breaking" the water droplets with higher frequency and thus obtaining smaller droplets with a larger distance between them. At smaller Oil/Water ratios, Rayleigh-Plateau instabilities start to appear and the water phase develops undulations. If this ratio descends to a limit, the water phase reaches a stable parallel regime flow, known as jetting, and the droplet formation is not achieved, which is in good agreement with theory [42,47].

The microdroplet formation in a T or Y-junction is a common topic of research and has been already discussed in detail [48,49]. From those studies it is known that diverse factors such as the geometry of the chip, dispersed solution viscosity or flow rates, as mentioned in the previous section, affect the size and shape of the droplets. Usually, in flow-focusing devices as the one presented here, the shearing responsible of the droplet formation is due to the relative magnitude of the co-flowing streams of the two immiscible liquids. In other words, the breakup in flow and droplet generation is the result of the competition between viscous stresses or shearing forces caused by the flow field and capillary stresses caused by the surface tension between phases. Numerically, the shearing force can be defined as the product of the average velocity ($u_c$) and the viscosity of the continuous phase ($\eta_c$) [50].

$$F_s = u_c \eta_c \tag{6}$$

The capillary stresses, for their part, can be defined in function of the surface tension ($\sigma$) and the diameter of the droplet ($D$) and they scale as $\sigma/D$ [51]. Then, the ratio of viscous-to-capillary stresses can be defined as follows:

$$Ca = \frac{u_c \eta_c D}{\sigma} \tag{7}$$

$Ca$ is known as the Capillary number, and it is a dimensionless number representing the ratio of viscous stress to interfacial tension and it is very useful to identify the droplet formation. For its part, in channels like the ones present in the microfluidic chips, the velocity gradient can be estimated as:

$$G \sim \frac{Q_c}{D_h^3} \tag{8}$$

Being $Q_c$ the flow rate of the continuous phase and $D_h$ the hydraulic diameter of the channel. So, taking into account these considerations, the relationship between the size of the droplet formed and the flow rate can be basically estimated by:

$$D \sim \frac{\sigma D_h^3}{\eta_c Q_c} \tag{9}$$

This expression demonstrates that the diameter of the final droplets increases inversely to the flow of the continuous phase, $Q_c$. Nevertheless, in the present case, the two immiscible phases are continuously injected at different flow rates so it is essential to define two new dimensionless parameters to characterize the droplet breakup: Ratio of flow rates ($\varphi = Q_d/Q_c$) and Viscosity ratio ($\alpha = \eta_d/\eta_c$). Subscripts $d$ and $c$ referring to dispersed and continuous phase, respectively. Numerous experimental and computational studies have delved into this topic and effectively confirmed this relationship [52–56]. Here, the chip design was fixed, the concentration of sodium alginate was maintained constant at 2 wt%, and the composition of the oil phase was the same in all experiments, so the viscosity ratio was invariable and the flow rates were the only factors to manipulate.

As shown in Fig. 6, different patterns of droplet generation could be differentiated depending on the flow rate ratio at a fixed $C_a$. At higher $Q$ values, droplets "break" at the junction due to the squeezing forces. When the value of $Q$ increases, the distance at which droplets pinch-off also gets bigger until becoming a continuous flow when $Q$ reaches the critical jetting value, where the oil and water streams co-flow parallelly without pinching. Simulations and the following studies are focused on the dripping regime so that they can be correlated with the experimental work.

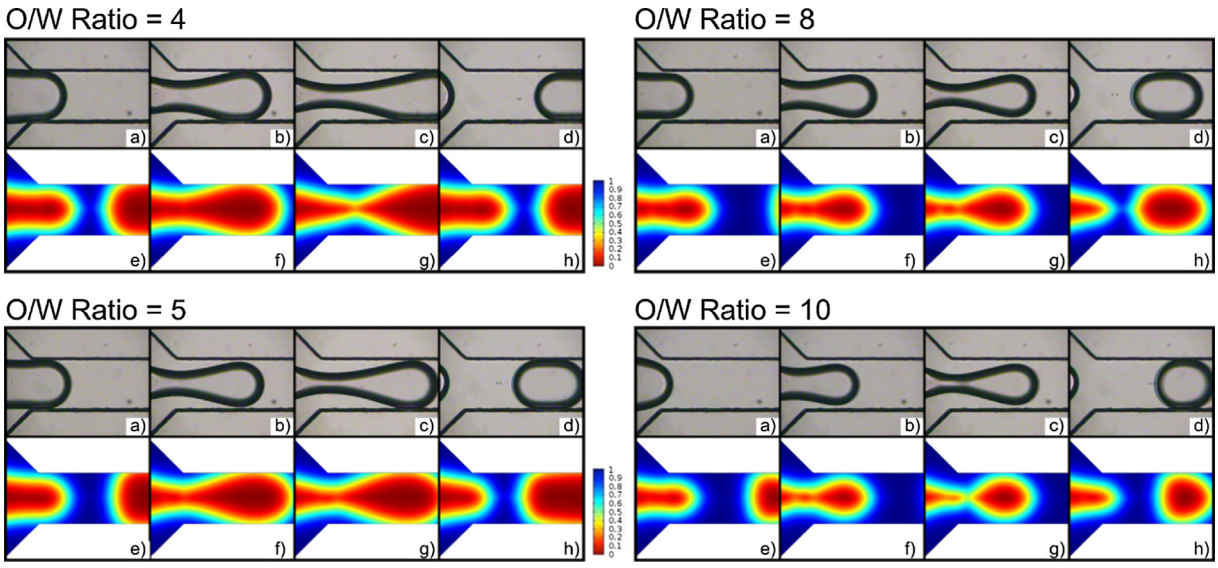


**Fig. 2.** Droplet generation inside the microchannels depending on the Oil/Water phase flow rate. Optical images of the experimental assays from a) to d), and their respective counterparts using COMSOL Multiphysics simulation software from e) to h). Colour legend corresponds to the molar fraction of oil phase.

Garteski et al. [57] postulated that, when the Capillary number is low enough, the final length of the droplets formed in T-junctions can be defined by two separated steps. First, the dispersed phase grows until blocking the continuous phase liquid. At this specific point the "blocking length" equals the width of the chip microchannels: $L_{block} = w_c$. Later, the continuous phase starts to apply a squeezing force to the dispersed stream. Under these circumstances the droplet keeps augmenting its length at rate $u_d = Q_d/(h \cdot w_c)$ and its volume at a rate $Q_d$. Then, if $d$ is defined as the characteristic width of the neck squeezing at a rate virtually equal to the velocity of the continuous phase ($u_c$); a new magnitude could be defined as "squeeze length": $L_{squeze} \approx d/u_c \cdot u_d = d \cdot Q_d/Q_c$. Having these considerations into account, the final length of the droplet ($L$) can be obtained by:

$$\frac{L}{w_c} = \frac{L_{block} + L_{squeze}}{w_c} = \frac{w_c + d \cdot Q_d/Q_c}{w_c} = 1 + \omega \cdot Q_d/Q_c = 1 + \omega \cdot \varphi \quad (10)$$

$L/w_c$ is known as the dimensionless length and $\omega$ is a fitting constant related to the thinning width. Data obtained by Garteski and co-workers fits well to this expression, nevertheless further studies served to improve the numerical characterization. Xu *et al.* [58] discovered that the "blocking length" $L_{block}$ and $w_c$ are not equal in every case, but they are dependent on the geometry ($L_{block}$=$\varepsilon \cdot w_c$). All things considered; a better approximation would be:

$$\frac{L}{w_c} = \varepsilon + \omega \cdot \varphi \quad (11)$$

being $\varepsilon$ a fitting constant that is related to the geometry of the microchannels.

Experimental measurements for a fixed $Ca_c = 0.0025$ resulted in monodisperse droplets created in a regular manner. As expected, the droplet length increased with $Q$ and started to show typical behaviours of the jetting regime when this value got close to 2. For this specific capillary number, experimental data fitted well to the scaling law exposed above. However, modifications in $Ca_c$ also provoked changes in the resulting fitting parameters. This fact clearly indicates that the $L/w_c$ is not only dependent on the flow rate ratio but also the Capillary number, being the $\varphi$ mainly responsible for the dynamic break-up of the interface and the $Ca_c$ playing an important role on the equilibrium between shear force of the continuous flow and interfacial force.

Recently Wu et al. [59] explored the droplet formation in microchannels following a similar approach and proposed that the nondimensional length of droplets $L/w_c$ exhibits a power-law dependence on the capillary number: $L/w_c = kCa_c^m$. This behaviour was previously reported by diverse authors, both in microfluidic cross-junctions [53,60] as well as in T-junctions [61]. Thus, the droplet size can be predicted by:

$$\frac{L}{w_c} = (\varepsilon + \omega \cdot \varphi) \cdot Ca_c^m \quad (12)$$

Data was adjusted to this model and values obtained for the fitting parameters were: $\varepsilon$ = 0.163, $\omega$ = 0.015 and $m$ = −0.209. The power-law exponent $m$ = −0.209 is very close to the experimental results obtained previously, both in T-junction [62] and cross-junction [59,60] geometries. To further test the validity of

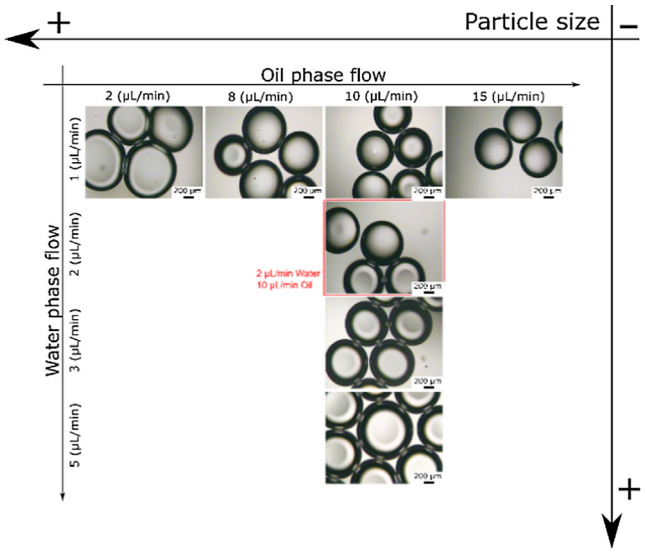


**Fig. 3.** Scheme illustrating the dependence between the water–oil flow ratio and the droplet size and distribution.

this scaling law, a parity plot was used, where the match between predicted and experimental values demonstrates its efficacy (S. M.5). Fig. 3 shows a diagram representing the relationship between sizes and flows supported with real optical images of the droplets (see Figs. 4 and 5).

As expected, mean size of the droplets increases inversely to the O/W ratio ($\varphi^{-1}$) and values are consistent with the numerical predictions. It is interesting to note that, due to the aforementioned fluctuations and instabilities in the channel flows when the ratio is too low or high, the homogeneity of the sizes notably decreases (see Table 2).

### 3.2. Gelation and formation of calcium alginate microparticles and chitosan-covered microspheres

After the droplet formation, alginate needs to crosslink with divalent ions in order to obtain a stable gelatinous substance. Recently, various methods for obtaining diverse polymeric alginate microparticles using microfluidic techniques have been developed. Fundamentally, the crosslinking reaction of alginate follows the equation:

$$2NaC_6H_7O_6 + CaCl_2 \rightarrow 2NaCl + CaC_{12}H_{14}O_{12}$$

Commonly, these hydrogel particles are generated by external [63–66] or internal gelation [67–71]. With internal gelation, the crosslinking starts, virtually, at the same time than the formation of the droplets [70,72]. This method is better to maintain a more evenly distributed and more homogeneous size and shape, resulting in particles with spherical structure. On the other hand, internal gelation is slower, as it depends on the diffusion of $Ca^{2+}$ ions from their centre to the surface [73], and what is more, the final particles tend to have a weak stiffness as the crosslinking is usually incomplete. Furthermore, the internal gelation method is way more sensitive, with a high degree of dependence on the initial concentrations and control of the process, since the particle solidification inside the microchip will provoke undesired fluctuations on the flow or clogging in microchannels. For its part, external gelation is typically achieved collecting the alginate droplets that are originated inside the microchip, in a gelation bath with a moderate-to-high concentration of calcium ions, leading to a crosslinking reaction of $Ca^{2+}$ and the carboxyl groups of alginate [66,67]. As the droplets get in contact with the bath, $Ca^{2+}$ ions start to diffuse through the droplets until obtaining fully crosslinked hydrogel microparticles. Due to the relatively high speed with which the crosslinking takes place, added to the gravitational and interfacial forces when they drip into the bath [63,64], the sphericity of the resulting particles is way more difficult to achieve, commonly obtaining pear-like or droplet-shaped morphologies with a wide size distribution [65,74,75]. The droplet falling in an immiscible liquid due to the gravitational forces is a typical object of study in fluid dynamics. Specifically, the behaviour of a deformable droplet in sedimentation processes has been well studied in previous works [76]. The deformation that the droplet interface suffers is a consequence of the stress in the flowing fluid. As it can be inferred from the numerical descriptions in the previous Section, both the Capillary number ($Ca$) and the Viscosity ratio ($\alpha$) are closely linked to this issue. Diverse mathematical characterizations [77] and experimental tests [78] have been conducted to prove and confirm the shape transition between the initial sphericity and the final tear-shaped or tailed morphology. Such a transformation is a dynamic change resulting from the competition between the viscous deformation and the opposite interfacial stresses that tend to restore the initial round shape. As exposed, when the sodium-alginate droplets get in contact with the $CaCl_2$ solution the ionic crosslinking reaction takes place almost instantly [79]. This quick solidification preserves the tear-shape morphology of the particles and provokes a notable rise in the microparticle density, accelerating the sedimentation process. Added to that, the quick gelation of the surface prevents the $Ca^{2+}$ ions from diffusing to the inner core, and, in this case, is the centre of the particles which is not completely solidified [80].

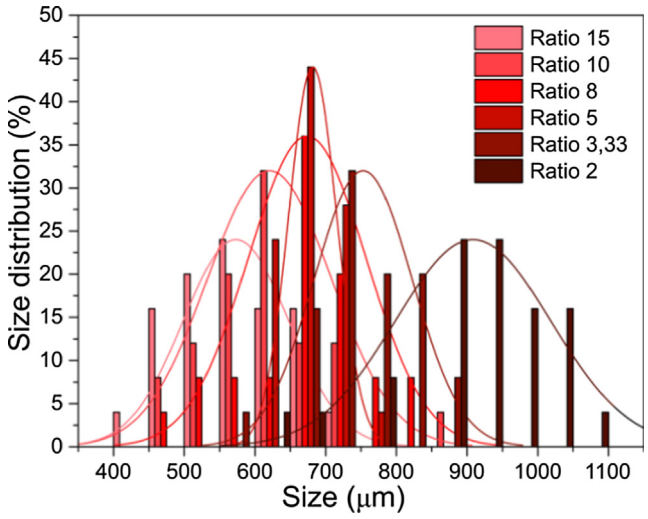


**Fig. 4.** Droplet size distribution at different Oil/Water ratios. A minimum amount of 40 droplets were measured for each condition.

In the more recent years, the interest in this topic of authors like Wang et al. [81] has led to new processes combining both internal and external gelation, solving partially the mentioned problems.

In the present case, Fig. 6, the procedure is a combination of internal gelation caused by the reaction between the $Ca^{2+}$ ions present in the HA surface and external, as the crosslinking process is completed in each respective collection bath. As explained, the gravitational and interfacial forces when the droplets drip into the first bath results in teardrop-shaped Ca-ALG microparticles (Fig. 7e)). In the second case, the addition of CHI and the acidic environment to the gelation bath provokes changes on the system properties. Values of Capillary number, Viscosity ratio or interfacial tension get modified, causing a rather different response. In this instance, the interfacial tension between the oil and water phases in the collecting bath is high enough to prevent the sodium alginate droplets from immersing in the bottom phase. Then, the crosslinking gets started while the droplets are still floating in the interface. Besides, chemical interactions occur between the two oppositely charged polymers creating fine fibrous Alg-Chi coacervates [82,83]. This electrostatic attraction creates a superficial layer of Chitosan around the spherical Alginate droplets. This layer slows down the diffusion of Calcium ions through the droplet, and when the weight of the solidifying droplets is high enough to surpass the interfacial tension and to submerge them into the water phase of the external bath, they have enough consistency to not get deformed by the stress caused by sedimentation flow. As one can appreciate on Fig. 7, resulting HMPs from this method exhibit a spherical core–shell structure, with presence of a fibrous surface that will play a major role diminishing the hydrogel degradation and modulating the delivery of drugs.

### 3.3. Kinetic adsorption assessment of Prop and Clox onto HA nanoparticles

Hydrogels are an encouraging solution for delivery of drugs such as small-molecule active principles or growth factors. Their suitability for these purposes is rooted in their capability to protect, deliver and locally release bioactive factors in a partially

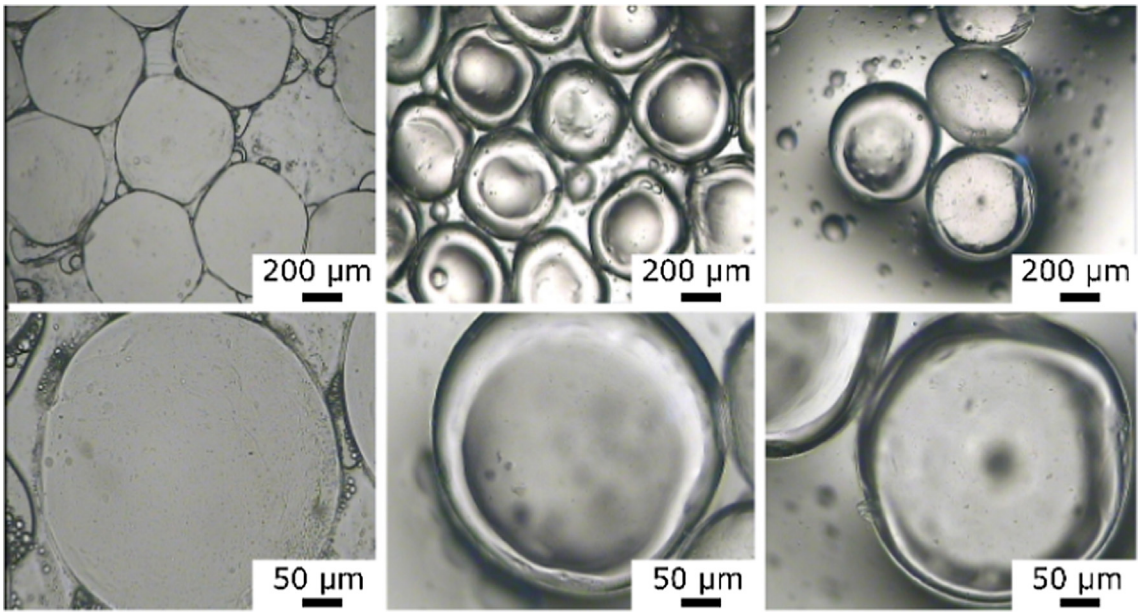


**Fig. 5.** Optical images of the Alginate droplets before crosslinking. It can be clearly seen that they maintain the spherical shape before they drip in the collecting bath.

**Table 2**
Size distribution. Mean and standard deviation.

| O/W Ratio | Mean Size (µm) | SD |
|---|---|---|
| 2 | 908,47 | 110.21 |
| 3.33 | 753.03 | 69.43 |
| 5 | 681.69 | 34.23 |
| 8 | 673.86 | 83.44 |
| 10 | 620.63 | 80.02 |
| 15 | 573.09 | 74.83 |

adjustable way [84], improving the results obtained by traditional drug-administration methods which usually need high and repeated dosage. The aforementioned advantages of the granular hydrogels over the bulk material are responsible for the growing use of HMP systems in delivery purposes. Their small sizes make them propitious for minimally invasive procedures using needles or catheters [85], and also, their versatility enables the possibility of combining various components, unifying multiple release profiles in a unique injection [22]. In this work, drug adsorption was performed onto the Hydroxyapatite nanoparticles. To analyze process, results were fitted to the Avrami's equation:

$$q_t = q_e\left(1 - e^{-[K_{av}\cdot t]^n}\right) \tag{13}$$

The relationship between time and adsorbed concentrations of Prop and Clox is depicted in Fig. 8. With a first quick glance at the curves it can already be noticed that both drugs follow a similar behaviour, reaching the adsorption equilibrium at around 2000 min. The results of the fittings for the order of the kinetic process ($n$) and its constant ($K_{sv}$) are shown in Table 3.

Data show a satisfactory fit with correlation coefficients close to 1. As observed, $n$ values for both drugs are low (0.2–0.8) suggesting that distribution of drug to the support is homogenous and adsorption does not occur with constant growth rate. At the same time, the values obtained for the $K_{sv}$ indicate that the adsorption, while relatively low in both cases, is notably higher in the case of Prop, probably due to the better affinity of this drug to the negatively charged surface of the hydroxyapatite nanorods (see Fig. 9).

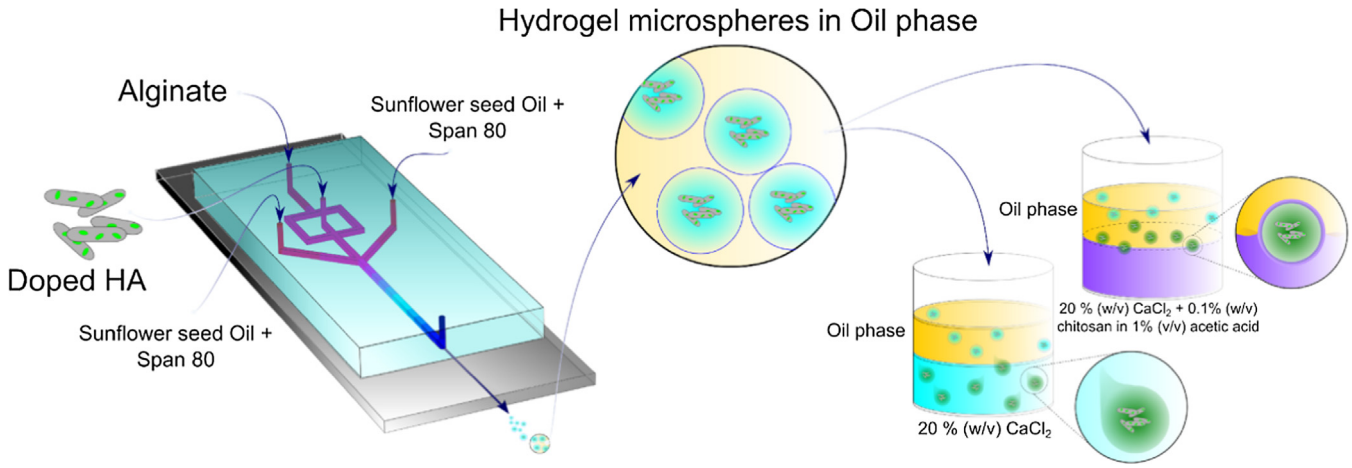


**Fig. 6.** Schematic representation of the microfluidic system used for obtaining hydrogel microparticles. Spherical droplets are formed before the collection in the gelation baths.

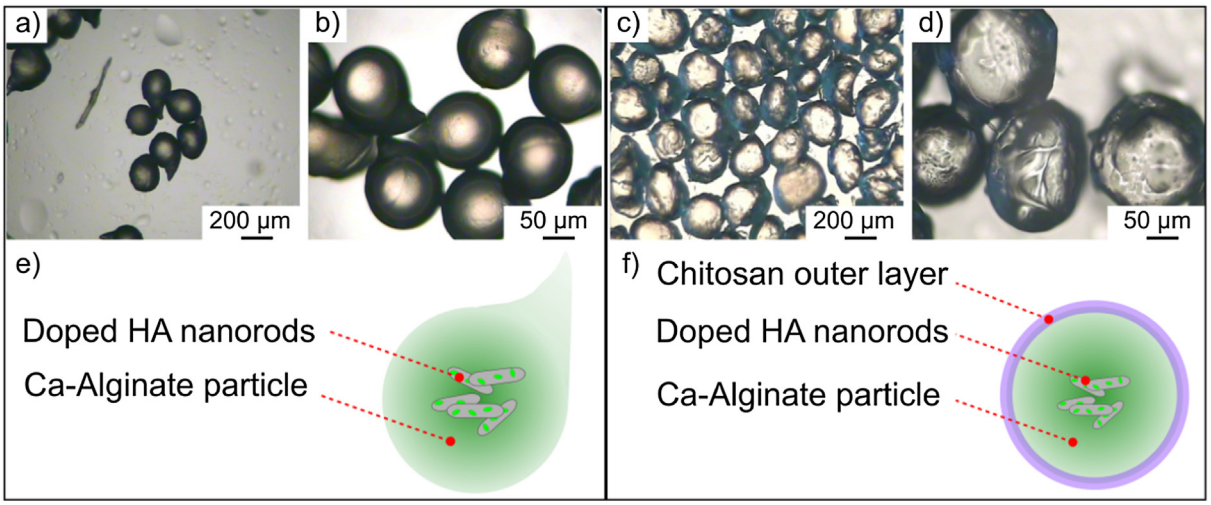


**Fig. 7.** a-b) Optical images of the crosslinked Ca-ALG microparticles. The teardrop shape can be clearly identified. c-d) Chitosan-covered microparticles. In this case, samples exhibit spherical or spheroid shape. All images were taken after crosslinking in the external gelation bath, and then filtered and dried with blotting paper. e-f) Schemes representing the two different microparticle shape and composition.

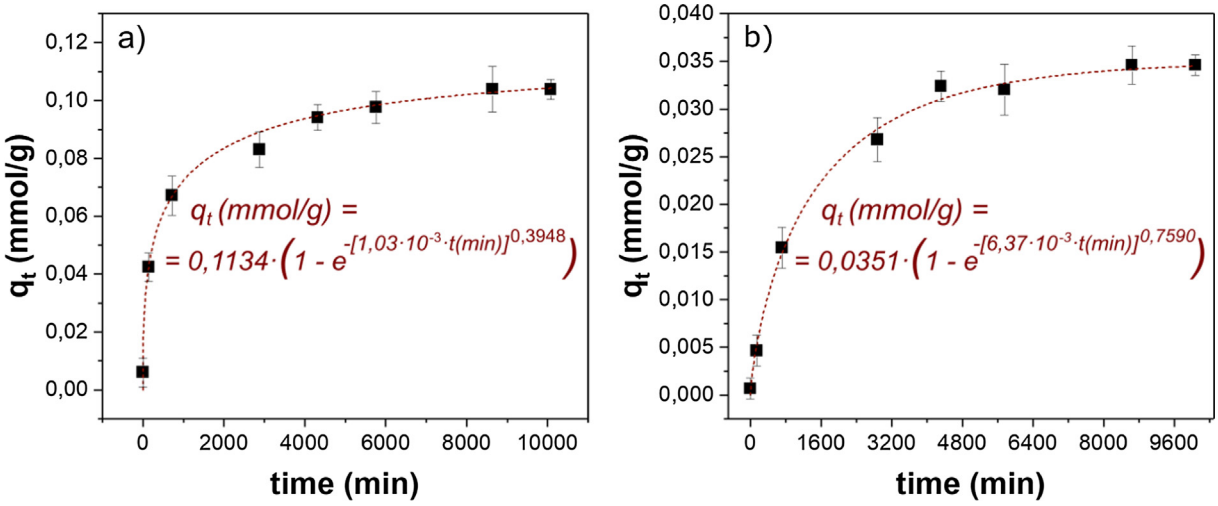


**Fig. 8.** Kinetic adsorption studies for a) Prop and b) Clox. Avrami's model at 37 °C.

**Table 3**
Kinetic adsorption parameters of Prop and Clox onto HA, obtained using Avrami equation at 37 °C.

| | $q_e$ (mmol/g) | $K_{av}$ ($min^{-1}$) | n | $R^2$ |
|---|---|---|---|---|
| Propanolol | 0.113 ± 0.014 | $1.03 \cdot 10^{-3} \pm 7.5 \cdot 10^{-4}$ | 0.394 ± 0.096 | 0.995 |
| Cloxacillin | 0.0350 ± 0.0010 | $6.37 \cdot 10^{-3} \pm 1.0 \cdot 10^{-4}$ | 0.758 ± 0.076 | 0.998 |

### 3.4. Desorption/release profiles

When a drug or an active principle is introduced in the inner matrix of a polymeric network, the consequential drug release is governed by the water transport. Hydrogels have distinctive and characteristic swelling kinetics, then; the so-called release by swelling-controlled mechanisms is mediated by the equilibrium between the drug diffusion through the polymer matrix and the opposite flow of water or biological fluid into the polymer. Initially, the drug is dispersed in the gel. Then, the solvent starts to evaporate at the same time as the dissolution medium penetrates the polymeric network, and the solvent-free polymer starts swelling. Therefore, depending on the relation of mobility between the dissolution media and the drug and the dynamics of polymer swelling, different transport profiles may appear: Fickian and non-Fickian or anomalous [86,87].

Following the theories proposed by Korsmayer – Peppas [88], the ratio between the amount of drug released to the medium at a time $t$ ($M_t$) and the total amount of drug released ($M_\infty$) can be approximated by an exponential expression, which describes the drug release from a matrix without taking into account the mechanisms of the release:

$$Q = \frac{M_t}{M_\infty} = kt^n \tag{14}$$

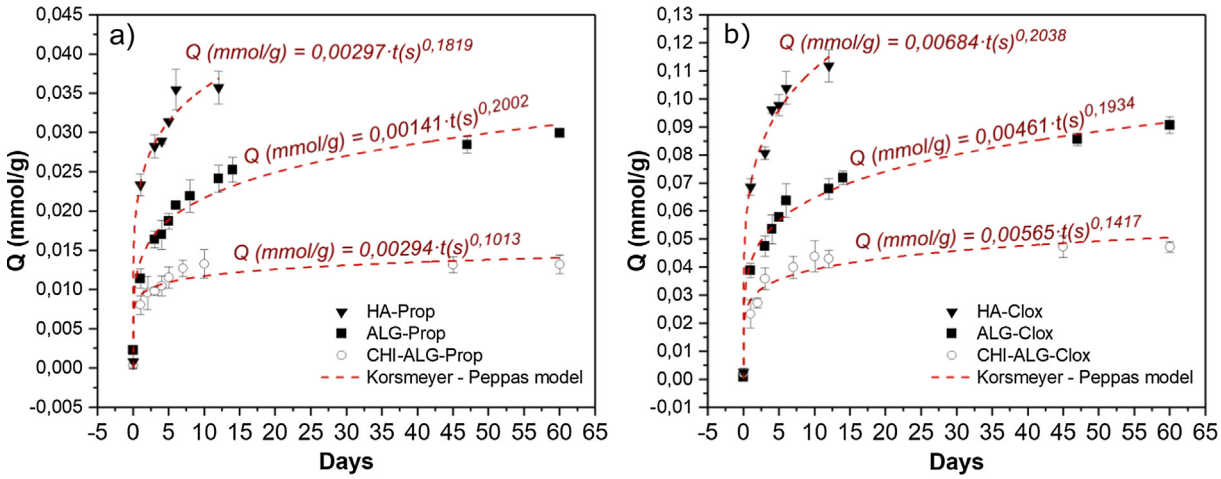


**Fig. 9.** Desorption studies a) Propranolol and, b) Cloxacillin. All data fit to Korsmeyer-Peppas model. The fitting expressions for each particular case are shown in the graph.

Thus, $M_t/M$ represents the fractional solute release by desorption at time t. k is a constant incorporating characteristics of drug and the macromolecular network system, and n is the diffusion exponent, which is indicative of the transport mechanism. All parameters are shown in Tables 5 and 6.

Peppas et al. have demonstrated that the morphology of the structure of release has a notable impact in the desorption process [41,88]. In the present case, as desorption occurs from nano-rods, tear-shaped morphologies and spheres, *n* values will depend on the relation between length and diameter. Apart from that, it should not be forgotten the fact that the homogeneity of the nano-rods in aqueous solution can be variable due to their instability and tendency to agglomerate. Furthermore, and based on their works, the first steps of the release are predominantly directed by the smaller particles, while the bigger ones have a more notable impact in the rest of the process. Having this into account it is safe to assure that the behaviour of the HA in water influence the whole desorption activity, which is probably why the diffusional exponent do not reach the values of $n = 0.451$ for Fickian release from cylinders and $n = 0.432$ for spheres that Peppas and coworkers reported [88]. Furthermore, it was also theoretically postulated [89] and experimentally probed [90] that values of *n* can get in the range ~0.2 due to irregularities on the particles shape. It is interesting to note that for both drugs, *n* is in the same range, suggesting that the transport mechanism is similar in the two cases, but the release rates are dependent on the crosslinking method. The desorption profiles of the particles alone was assessed as well for comparative purposes. In the case of the nano-rods alone, the total desorption occurs within 7 days for both drugs. On the contrary when the particles are wrapped in the hydrogel matrix, the stability in water of crosslinked alginate and chitosan prevents the drugs from be released to the media. As Tables 4, 5, and 6 show, within the time range studied, 60 days, Chi-covered spheres have a cumulative release of 38.31% and 45.46% for Prop and Clox, respectively; while values for Alginate tear-shaped particles are substantially higher reaching 87.27%. The fibrous surface arising from the electrostatic interactions between Chitosan and Alginate effectively slows down the release by hampering the diffusion of the drug into the dissolution medium. This fact highlights the versatility of this kind of complex hybrid HMPs that can be manipulated in order to regulate the release behaviour. Further studies are on their way to improve the release response and to develop granular hydrogels from the obtained HMPs. The properties and knowledge arising from this study of the micro and nanoscale structures will be decisive in understanding the response of the macroscale constructions on the human body.

**Table 4**
Cumulative in vitro release of Propranolol and Cloxacillin from HA nanoparticles, ALG micropartiles and CHI-ALG microspheres.

| | Cumulative Release |
|---|---|
| HA-Prop | 100.00% |
| ALG-Prop | 86.60% |
| CHI-ALG-Prop | 38.31% |
| HA-Clox | 100.00% |
| ALG-Clox | 87.27% |
| CHI-ALG-Clox | 45.46% |

**Table 5**
Desorption studies for Prop. Parameters of Korsmeyer – Peppas model for the three different samples.

| | K ($s^{-1}$) | n | $R^2$ |
|---|---|---|---|
| HA-Prop | $(3.0 \pm 1.2) \cdot 10^{-3}$ | 0.181 ± 0.030 | 0.985 |
| ALG-Prop | $(1.41 \pm 0.39) \cdot 10^{-3}$ | 0.200 ± 0.020 | 0.962 |
| CHI-ALG-Prop | $(2.94 \pm 0.86) \cdot 10^{-3}$ | 0.101 ± 0.021 | 0.944 |

**Table 6**
Desorption studies for Clox. Parameters of Korsmeyer – Peppas model for the three different samples.

| | K ($s^{-1}$) | n | $R^2$ |
|---|---|---|---|
| HA-Clox | $(6.8 \pm 2.3) \cdot 10^{-3}$ | 0.203 ± 0.026 | 0.989 |
| ALG-Clox | $(4.61 \pm 0.75) \cdot 10^{-3}$ | 0.193 ± 0.011 | 0.990 |
| CHI-ALG-Clox | $(5.6 \pm 2.0) \cdot 10^{-3}$ | 0.142 ± 0.026 | 0.942 |

## 4. Conclusions

In this work, two different types of green, sustained and multifaceted HMPs have been created using Chitosan, Alginate and drug doped Hydroxyapatite. Results from the computer modelling were in a notable accordance with the real behaviour of the two immiscible phases and allowed to demonstrate the dependency between flow ratios and geometry of the microchip with the final sizes and shapes of the obtained HMPs. This relationship has been further confirmed both numerically and experimentally with outstanding reliability. For its part, the combination of internal and different compositions of an external bath has been proved to be highly useful for manipulating the morphologies and for obtaining a superior

degree of homogeneity. Finally, the assessment of drug loading and delivery using specific models reveals that drug delivery ratios can be partially controlled depending on the structures designed and the applications purposed. The promising properties of obtained hydrogel microparticles make them a more than adequate candidate for the construction of diverse granular hydrogels with numerous tissue engineering applications, promoting bone healing while avoiding bacterial infection.

## CRediT authorship contribution statement

**Ramón Rial:** Conceptualization, Methodology, Investigation, Software, Formal analysis. **Natalia Hassan:** Conceptualization, Data curation, Supervision. **Zhen Liu:** Visualization, Formal analysis, Writing – review & editing. **Juan M. Ruso:** Conceptualization, Supervision, Project administration.

## Declaration of Competing Interest

The authors declare that they have no known competing financial interests or personal relationships that could have appeared to influence the work reported in this paper.

## Acknowledgements

The authors acknowledge Ministerio de Ciencia e Innovacion (PID2019-111327GB-100). N. H. thanks Proyecto FONDECYT de Iniciación (11170849) and FONDAP (15130011).

## Appendix A. Supplementary material

Supplementary data to this article can be found online at https://doi.org/10.1016/j.molliq.2021.117598.

## References

[1] Q. Zou, Y. Li, L. Zhang, Y. Zuo, J. Li, J. Li, Antibiotic delivery system using nano-hydroxyapatite/chitosan bone cement consisting of berberine, J. Biomed. Mater. Res. Part A 89A (2009) 1108–1117.
[2] C. Zhang, C. Li, S. Huang, Z. Hou, Z. Cheng, P. Yang, et al., Self-activated luminescent and mesoporous strontium hydroxyapatite nanorods for drug delivery, Biomaterials 31 (2010) 3374–3383.
[3] R. Gadow, A. Killinger, N. Stiegler, Hydroxyapatite coatings for biomedical applications deposited by different thermal spray techniques, Surf. Coat. Technol. 205 (2010.) 1157–1164.
[4] L. Benedini, J. Laiuppa, G. Santillán, M. Baldini, P. Messina, Antibacterial alginate/nano-hydroxyapatite composites for bone tissue engineering: Assessment of their bioactivity, biocompatibility, and antibacterial activity, Mater. Sci. Eng., C 115 (2020) 111101.
[5] D.J.A. Netz, P. Sepulveda, V.C. Pandolfelli, A.C.C. Spadaro, J.B. Alencastre, M.V.L. B. Bentley, J.M. Marchetti, Potential Use of Gelcasting Hydroxyapatite Porous Ceramic as an Implantable Drug Delivery System, Int. J. Pharm. 213 (1-2) (2001) 117–125.
[6] A. Uchida, Y. Shinto, N. Araki, K. Ono, Slow release of anticancer drugs from porous calcium hydroxyapatite ceramic, J. Orthop. Res. 10 (3) (1992) 440–445.
[7] M. Rivas, L.J. del Valle, A.M. Rodríguez-Rivero, P. Turon, J. Puiggalí, C. Alemán, Loading of Antibiotic into Biocoated Hydroxyapatite Nanoparticles: Smart Antitumor Platforms with Regulated Release, ACS Biomater. Sci. Eng. 4 (9) (2018) 3234–3245.
[8] A. Nokhodchi, A. Tailor, In situ cross-linking of sodium alginate with calcium and aluminum ions to sustain the release of theophylline from polymeric matrices, Il Farmaco 59 (12) (2004) 999–1004.
[9] K.S. Katti, D.R. Katti, R. Dash, Synthesis and characterization of a novel chitosan/montmorillonite/hydroxyapatite nanocomposite for bone tissue engineering, Biomed. Mater. 3 (2008) 034122.
[10] J. Venkatesan, I. Bhatnagar, P. Manivasagan, K.-H. Kang, S.-K. Kim, Alginate composites for bone tissue engineering: A review, Int. J. Biol. Macromol. 72 (2015) 269–281.
[11] H. Luo, G. Zuo, G. Xiong, C. Li, C. Wu, Y. Wan, Porous nanoplate-like hydroxyapatite–sodium alginate nanocomposite scaffolds for potential bone tissue engineering, Mater. Technol. 32 (2) (2017) 78–84.
[12] M. Nakauma, T. Funami, Y. Fang, K. Nishinari, K.I. Draget, G.O. Phillips, Calcium binding and calcium-induced gelation of sodium alginate modified by low molecular-weight polyuronate, Food Hydrocolloids 55 (2016) 65–76.
[13] P. Sharma, N. Sharma, O. Pal, R. Malviya, Applications of Chitosan and Chitosan Derivatives in Drug Delivery, Adv. Biolog. Res. 5 (2011) 28–37.
[14] M. Gomez-Florit, A. Pardo, R.M.A. Domingues, A.L. Graça, P.S. Babo, R.L. Reis, M. E. Gomes, Natural-Based Hydrogels for Tissue Engineering Applications, Molecules 25 (24) (2020) 5858, https://doi.org/10.3390/molecules25245858.
[15] S.M. Bakht, A. Pardo, M. Gómez-Florit, R.L. Reis, R.M.A. Domingues, M.E. Gomes, Engineering next-generation bioinks with nanoparticles: moving from reinforcement fillers to multifunctional nanoelements, J. Mater. Chem. B 9 (2021) 5025–5038.
[16] A. Pardo, M. Gómez-Florit, S. Barbosa, P. Taboada, R.M.A. Domingues, M.E. Gomes, Magnetic Nanocomposite Hydrogels for Tissue Engineering: Design Concepts and Remote Actuation Strategies to Control Cell Fate, ACS Nano 15 (1) (2021) 175–209.
[17] F. Heidari, M.E. Bahrololoom, D. Vashaee, L. Tayebi, In situ preparation of iron oxide nanoparticles in natural hydroxyapatite/chitosan matrix for bone tissue engineering application, Ceram. Int. 41 (2015) 3094–3100.
[18] R. Rial, Z. Liu, J.M. Ruso, Soft Actuated Hybrid Hydrogel with Bioinspired Complexity to Control Mechanical Flexure Behavior for Tissue Engineering, Nanomaterials 10 (7) (2020) 1302, https://doi.org/10.3390/nano10071302.
[19] J. Venkatesan, I. Bhatnagar, S.-K. Kim, Chitosan-alginate biocomposite containing fucoidan for bone tissue engineering, Mar Drugs 12 (1) (2014) 300–316.
[20] J. Yan, Y. Miao, H. Tan, T. Zhou, Z. Ling, Y. Chen, X. Xing, X. Hu, Injectable alginate/hydroxyapatite gel scaffold combined with gelatin microspheres for drug delivery and bone tissue engineering, Mater. Sci. Eng., C 63 (2016) 274–284.
[21] A.C. Daly, L. Riley, T. Segura, J.A. Burdick, Hydrogel microparticles for biomedical applications, Nat. Rev. Mater. 5 (1) (2020) 20–43.
[22] J.E. Mealy, J.J. Chung, H.-H. Jeong, D. Issadore, D. Lee, P. Atluri, et al., Injectable Granular Hydrogels with Multifunctional Properties for Biomedical Applications, Adv. Mater. 30 (2018) 1705912.
[23] E. Sideris, D.R. Griffin, Y. Ding, S. Li, W.M. Weaver, D. Di Carlo, et al., Particle Hydrogels Based on Hyaluronic Acid Building Blocks, ACS Biomater. Sci. Eng. 2 (2016) 2034–2041.
[24] E.K. Sackmann, A.L. Fulton, D.J. Beebe, The present and future role of microfluidics in biomedical research, Nature 507 (7491) (2014) 181–189.
[25] T.M. Squires, S.R. Quake, Microfluidics: Fluid physics at the nanoliter scale, Rev. Modern Phys. 77 (2005) 977–1026.
[26] G.M. Whitesides, The origins and the future of microfluidics, Nature 442 (7101) (2006) 368–373.
[27] B.G. Chung, K.-H. Lee, A. Khademhosseini, S.-H. Lee, Microfluidic fabrication of microengineered hydrogels and their application in tissue engineering, Lab Chip 12 (1) (2012) 45–59.
[28] Y.-S. Torisawa, C.S. Spina, T. Mammoto, A. Mammoto, J.C. Weaver, T. Tat, J.J. Collins, D.E. Ingber, Bone marrow-on-a-chip replicates hematopoietic niche physiology in vitro, Nat. Methods 11 (6) (2014) 663–669.
[29] C.-X. Zhao, Multiphase flow microfluidics for the production of single or multiple emulsions for drug delivery, Adv. Drug Deliv. Rev. 65 (2013) 1420–1446.
[30] F.S. Majedi, M.M. Hasani-Sadrabadi, S. Hojjati Emami, M.A. Shokrgozar, J.J. VanDersarl, E. Dashtimoghadam, A. Bertsch, P. Renaud, Microfluidic assisted self-assembly of chitosan based nanoparticles as drug delivery agents, Lab Chip 13 (2) (2013) 204–207.
[31] M.T. Guo, A. Rotem, J.A. Heyman, D.A. Weitz, Droplet microfluidics for high-throughput biological assays, Lab Chip 12 (2012) 2146–2155.
[32] R. Rial, P.G. Tahoces, N. Hassan, M.L. Cordero, Z. Liu, J.M. Ruso, Noble microfluidic system for bioceramic nanoparticles engineering, Mater. Sci. Eng., C 102 (2019) 221–227.
[33] R. Rial, J.F.A. Soltero, P.V. Verdes, Z. Liu, J.M. Ruso, Mechanical Properties of Composite Hydrogels for Tissue Engineering, Curr Top Med Chem 18 (2018) 1214–1223.
[34] R.G. Larson, The Structure and Rheology of Complex Fluids, Oxford University Press, New York, 1999.
[35] P. Decuzzi, B. Godin, T. Tanaka, S.-Y. Lee, C. Chiappini, X. Liu, M. Ferrari, Size and shape effects in the biodistribution of intravascularly injected particles, J. Control. Release 141 (3) (2010) 320–327.
[36] J.A. Champion, Y.K. Katare, S. Mitragotri, Particle shape: A new design parameter for micro- and nanoscale drug delivery carriers, J. Control. Release 121 (1-2) (2007) 3–9.
[37] B.B. Mendes, M. Gómez-Florit, A.G. Hamilton, M.S. Detamore, R.M.A. Domingues, R.L. Reis, et al., Human platelet lysate-based nanocomposite bioink for bioprinting hierarchical fibrillar structures, Biofabrication 12 (2019) 015012.
[38] Y. Hu, Q. Wang, J. Wang, J. Zhu, H. Wang, Y. Yang, Shape controllable microgel particles prepared by microfluidic combining external ionic crosslinking, Biomicrofluidics 6 (2012) 26502–265029.
[39] Y. Guesmi, H. Agougui, R. Lafi, M. Jabli, A. Hafiane, Synthesis of hydroxyapatite-sodium alginate via a co-precipitation technique for efficient adsorption of Methylene Blue dye, J. Mol. Liq. 249 (2018) 912–920.
[40] M. Avrami, Granulation, Phase Change, and Microstructure Kinetics of Phase Change. III, J. Chem. Phys. 9 (2) (1941) 177–184.
[41] N.A. Peppas, A model of dissolution-controlled solute release from porous drug delivery polymeric systems, J Biomed Mater Res 17 (1983) 1079–1087.
[42] C.N. Baroud, F. Gallaire, R. Dangla, Dynamics of microfluidic droplets, Lab Chip 10 (2010) 2032–2045.

[43] V. Daru, Level Set Methods and Fast Marching Methods – Evolving Interfaces in Computational Geometry, Fluid Mechanics, Computer Vision, and Materials Science by J.A. Sethian (Cambridge University Press, Cambridge, UK, 1999, 2nd edition, 378 pp.) £18.95 paperback ISBN 0 521 64557 3, Eur. J. Mechanics - B/Fluids 19 (2000) 531–532.
[44] L.R. Fisher, E.E. Mitchell, N.S. Parker, Interfacial Tensions of Commercial Vegetable Oils with Water, J. Food Sci. 50 (2006) 1201–1202.
[45] J.M. Marques Junior, A.L.H. Muller, E.L. Foletto, A.B. da Costa, C.A. Bizzi, E. Irineu Muller, Determination of Propranolol Hydrochloride in Pharmaceutical Preparations Using Near Infrared Spectrometry with Fiber Optic Probe and Multivariate Calibration Methods, J. Anal. Methods Chem. 2015 (2015.) 795102.
[46] J. Malakar, A.K. Nayak, D. Pal, Development of cloxacillin loaded multiple-unit alginate-based floating system by emulsion-gelation method, Int. J. Biol. Macromol. 50 (1) (2012) 138–147.
[47] A.S. Utada, A. Fernandez-Nieves, H.A. Stone, D.A. Weitz, Dripping to Jetting Transitions in Coflowing Liquid Streams, Phys. Rev. Lett. 99 (2007).
[48] I.-L. Ngo, T.-D. Dang, C. Byon, S.W. Joo, A numerical study on the dynamics of droplet formation in a microfluidic double T-junction, Biomicrofluidics 9 (2015) 024107.
[49] F.Y. Ushikubo, F.S. Birribilli, D.R.B. Oliveira, R.L. Cunha, Y- and T-junction microfluidic devices: effect of fluids and interface properties and operating conditions, Microfluid. Nanofluid. 17 (4) (2014) 711–720.
[50] K. Wang, Y.C. Lu, J.H. Xu, G.S. Luo, Droplet generation in micro-sieve dispersion device, Microfluid. Nanofluid. 10 (2011) 1087–1095.
[51] V. Cristini, Y.-C. Tan, Theory and numerical simulation of droplet dynamics in complex flows - A review, Lab Chip 4 (4) (2004) 257–264.
[52] P. Garstecki, M.J. Fuerstman, H.A. Stone, G.M. Whitesides, Formation of droplets and bubbles in a microfluidic T-junction—scaling and mechanism of break-up, Lab Chip 6 (3) (2006) 437, https://doi.org/10.1039/b510841a.
[53] J. Tan, J.H. Xu, S.W. Li, G.S. Luo, Drop dispenser in a cross-junction microfluidic device: Scaling and mechanism of break-up, Chem. Eng. J. 136 (2-3) (2008) 306–311.
[54] T. Fu, Y. Ma, D. Funfschilling, H.Z. Li, Bubble formation and breakup mechanism in a microfluidic flow-focusing device, Chem. Eng. Sci. 64 (2009) 2392–2400.
[55] M. DE MENECH, P. GARSTECKI, F. JOUSSE, H.A. STONE, Transition from squeezing to dripping in a microfluidic T-shaped junction, J. Fluid Mech. 595 (2008) 141–161.
[56] H. Liu, Y. Zhang, Droplet formation in a T-shaped microfluidic junction, J. Appl. Phys. 106 (2009) 034906.
[57] P. Garstecki, M.J. Fuerstman, H.A. Stone, G.M. Whitesides, Formation of droplets and bubbles in a microfluidic T-junction - Scaling and mechanism of break-up, Lab Chip 6 (3) (2006) 437, https://doi.org/10.1039/b510841a.
[58] J.H. Xu, S.W. Li, J. Tan, G.S. Luo, Correlations of droplet formation in T-junction microfluidic devices: from squeezing to dripping, Microfluid. Nanofluid. 5 (6) (2008) 711–717.
[59] S. Wu, J. Chen, X. Liu, F. Yao, Experimental study of droplet formation in the cross-junction, J. Dispersion Sci. Technol. 42 (8) (2021) 1233–1240.
[60] H. Liu, Y. Zhang, Droplet formation in microfluidic cross-junctions, Phys. Fluids 23 (2011) 082101.
[61] J. Tan, S.W. Li, K. Wang, G.S. Luo, Gas–liquid flow in T-junction microfluidic devices with a new perpendicular rupturing flow route, Chem. Eng. J. 146 (3) (2009) 428–433.
[62] G.F. Christopher, N.N. Noharuddin, J.A. Taylor, S.L. Anna, Experimental observations of the squeezing-to-dripping transition in T-shaped microfluidic junctions, Phys. Rev. E 78 (2008).
[63] L. Capretto, S. Mazzitelli, C. Balestra, A. Tosi, C. Nastruzzi, Effect of the gelation process on the production of alginate microbeads by microfluidic chip technology, Lab Chip 8 (4) (2008) 617, https://doi.org/10.1039/b714876c.
[64] T.D. Dang, S.W. Joo, Preparation of tadpole-shaped calcium alginate microparticles with sphericity control, Colloids Surf., B 102 (2013) 766–771.
[65] Y.-S. Lin, C.-H. Yang, Y.-Y. Hsu, C.-L. Hsieh, Microfluidic synthesis of tail-shaped alginate microparticles using slow sedimentation, Electrophoresis 34 (3) (2013) 425–431.
[66] C.-H. Yeh, Q. Zhao, S.-J. Lee, Y.-C. Lin, Using a T-junction microfluidic chip for monodisperse calcium alginate microparticles and encapsulation of nanoparticles, Sens. Actuators, A 151 (2) (2009) 231–236.
[67] S.H. Ching, N. Bansal, B. Bhandari, Alginate gel particles–A review of production techniques and physical properties, Crit. Rev. Food Sci. Nutr. 57 (6) (2017) 1133–1152.
[68] K. Liu, H.-J. Ding, J. Liu, Y. Chen, X.-Z. Zhao, Shape-Controlled Production of Biodegradable Calcium Alginate Gel Microparticles Using a Novel Microfluidic Device, Langmuir 22 (2006) 9453–9457.
[69] W.H.T. Tan, S. Takeuchi, Monodisperse Alginate Hydrogel Microbeads for Cell Encapsulation, Adv. Mater. 19 (2007) 2696–2701.
[70] V. Workman, S. Dunnett, P. Kille, D. Palmer, On-Chip Alginate Microencapsulation of Functional Cells, Macromol. Rapid Commun. 29 (2008) 165.
[71] J.H. Xu, S.W. Li, J. Tan, G.S. Luo, Controllable Preparation of Monodispersed Calcium Alginate Microbeads in a Novel Microfluidic System, Chem. Eng. Technol. 31 (2008) 1223–1226.
[72] E. Amici, G. Tetradis-Meris, C.P. de Torres, F. Jousse, Alginate gelation in microfluidic channels, Food Hydrocolloids 22 (1) (2008) 97–104.
[73] E. Tumarkin, E. Kumacheva, Microfluidic generation of microgels from synthetic and natural polymers, Chem. Soc. Rev. 38 (2009) 2161–2168.
[74] L. Mazutis, R. Vasiliauskas, D.A. Weitz, Microfluidic Production of Alginate Hydrogel Particles for Antibody Encapsulation and Release, Macromol Biosci 15 (2015) 1641–1646.
[75] A.K.A.S. Brun-Graeppi, C. Richard, M. Bessodes, D. Scherman, O.-W. Merten, Cell microcarriers and microcapsules of stimuli-responsive polymers, J. Control. Release 149 (3) (2011) 209–224.
[76] I. Smagin, M. Pathak, O.M. Lavrenteva, A. Nir, Motion and shape of an axisymmetric viscoplastic drop slowly falling through a viscous fluid, Rheol. Acta 50 (4) (2011) 361–374.
[77] A. Potapov, R. Spivak, O.M. Lavrenteva, A. Nir, Motion and deformation of drops in Bingham fluid, Ind. Eng. Chem. Res. 45 (2006) 6985–6995.
[78] O.M. Lavrenteva, Y. Holenberg, A. Nir, Motion of viscous drops in tubes filled with yield stress fluid, Chem. Eng. Sci. 64 (2009) 4772–4786.
[79] H. Zhang, E. Tumarkin, R. Peerani, Z. Nie, R.M.A. Sullan, G.C. Walker, et al., Microfluidic Production of Biopolymer Microcapsules with Controlled Morphology, J. Am. Chem. Soc. 128 (2006) 12205–12210.
[80] T. Braschler, A. Valero, L. Colella, K. Pataky, J. Brugger, P. Renaud, Link between Alginate Reaction Front Propagation and General Reaction Diffusion Theory, Anal. Chem. 83 (2011) 2234–2242.
[81] Q. Wang, S. Liu, H. Wang, J. Zhu, Y. Yang, Alginate droplets pre-crosslinked in microchannels to prepare monodispersed spherical microgels, Colloids Surf., A 482 (2015) 371–377.
[82] X. Meng, F. Tian, J. Yang, C.-N. He, N. Xing, F. Li, Chitosan and alginate polyelectrolyte complex membranes and their properties for wound dressing application, J. Mater. Sci. - Mater. Med. 21 (2010) 1751–1759.
[83] L. Becherán-Marón, C. Peniche, W. Argüelles-Monal, Study of the interpolyelectrolyte reaction between chitosan and alginate: influence of alginate composition and chitosan molecular weight, Int. J. Biol. Macromol. 34 (1-2) (2004) 127–133.
[84] T.R. Hoare, D.S. Kohane, Hydrogels in drug delivery: Progress and challenges, Polymer 49 (2008) 1993–2007.
[85] D.R. Griffin, W.M. Weaver, P.O. Scumpia, D. Di Carlo, T. Segura, Accelerated wound healing by injectable microporous gel scaffolds assembled from annealed building blocks, Nat. Mater. 14 (2015) 737–744.
[86] J. Crank, The Mathematics of Diffusion, Oxford University Press, 1979.
[87] J.A. Ferreira, M. Grassi, E. Gudiño, P. de Oliveira, A new look to non-Fickian diffusion, Appl. Math. Model. 39 (1) (2015) 194–204.
[88] P.L. Ritger, N.A. Peppas, A simple equation for description of solute release I. Fickian and non-fickian release from non-swellable devices in the form of slabs, spheres, cylinders or discs, J. Control. Release 5 (1) (1987) 23–36.
[89] N.A. Peppas, A.R. Khare, Preparation, structure and diffusional behavior of hydrogels in controlled release, Adv. Drug Deliv. Rev. 11 (1-2) (1993) 1–35.
[90] S.A. Agnihotri, T.M. Aminabhavi, Controlled release of clozapine through chitosan microparticles prepared by a novel method, J. Control. Release 96 (2004) 245–259.